On-Chip Stimulated Brillouin Scattering to Linearize a Dual-Parallel Mach–Zehnder Modulator

Cristina Catalá-Lahoz, Moritz Merklein, Choon Kong Lai, Duk-Yong Choi, Stephen J. Madden, Benjamin J. Eggleton, *Fellow, IEEE*, and José Capmany, *Fellow, IEEE*

***Abstract*—Microwave photonics offers great potential for wideband systems, but link linearity remains limited and must be overcome to have the dynamic range required for many applications. Here, we propose and demonstrate the linearization of a Dual-Parallel Mach-Zehnder Modulator by frequency-selectively controlling the phase and amplitude of the carrier utilizing a dual-pump, narrowband stimulated Brillouin scattering scheme. Measurements using a single-mode fiber and chalcogenide waveguides on a chip are presented. As a result, a suppression of third-order distortion terms of 27 dB is experimentally obtained, and a spurious free dynamic range improvement of 9 dB using fiber and 4.5 dB using a chalcogenide chip, respectively. On-chip measurements enable the possibility of a fully integrated system, significantly reducing the overall footprint.**

***Index Terms*—Brillouin scattering, integrated optics, linearization, microwave photonics, nonlinear optics.**

I. Introduction

MICROWAVE photonic links (MPLs) are broadly used in applications such as radar systems, wireless communications, and satellite links [1], [2]. These systems exploit the inherent advantages of photonics, including wide bandwidth, immunity to electromagnetic interference, and low propagation loss in optical waveguides [3]. However, one of the primary limitations of MPLs lies in their susceptibility to non-linear distortions, which degrade signal quality and overall system performance [4]. Among these distortions, third-order intermodulation distortion (IMD3) terms are especially problematic, as they can interfere with the desired signal and reduce the spurious free dynamic range (SFDR) of the system. The electro-optic modulator, a critical component of MPLs, is often the dominant source of IMD3 terms, making its linearization a key focus for performance improvement.

Various strategies have been developed to address the challenges of non-linear distortions in MPLs, ranging from advanced modulation schemes to optical signal processing techniques [5], [6]. Early efforts focused on employing additional electro-optic modulators, arranged in series or parallel, to generate complementary IMD3 terms, which could cancel the distortions introduced by the primary modulator at the photodetector (PD) [7]. Another effective technique involves optical spectrum processing, where the optical carrier band (OCB) and optical sidebands (OSB) are selectively tuned to suppress IMD3 terms [8], [9]. Initially demonstrated for intensity modulation, this method showed that applying a phase shift to the optical carrier could suppress IMD3 terms in standard MZMs. Later developments extended the approach to phase modulators (PMs), which offer advantages such as lower loss and simplicity but require more intricate optical spectrum processing to manage both phase and amplitude of the sidebands.

More complex modulators such as Dual-Parallel Mach-Zenhder Modulator (DPMZMs) have been studied for linearization. The techniques include optimizing the power balance between electrical drive signals [10], fine-tuning input and output optical splitting ratios [11], and adjusting the operating points of single-drive configurations [12]. Additional techniques involve active control of the RF input through carefully designed electrical phase shifters [13], leveraging complementary IMD3 terms within individual modulators [14] or using secondary DPMZMs arranged in polarization-multiplexed configurations [15]. Lastly, combining a DPMZM and optical processing techniques is another way to address the challenge posed by IMD3 terms and improve the MPL linearity [16]. This method aims to enhance linearity by selectively manipulating the amplitude and phase of the optical carrier. However, this technique has stringent requirements for the optical processing function, i.e. it needs to be narrowband to affect only the optical carrier and not the sidebands and needs to be able to control amplitude and phase. Programmable filters used to manipulate the amplitude and phase of the carrier are bulky systems and have a minimum bandwidth of 10 GHz, which limits the lower modulation frequencies that are close to the carrier. Furthermore, optical

Received 26 December 2024; revised 18 February 2025; accepted 26 February 2025. Date of publication 28 February 2025; date of current version 2 June 2025. This work was supported in part by the Generalitat Valenciana Project under Grant PROMETEO/2021/015, in part by Australian National Fabrication Facility (ANFF) OptoFab ACT Node, in part by Australian Research Council under Grant DP220101431, and in part by the Australian Research Council Center of Excellence in Optical Microcombs for Breakthrough Science under Grant CE230100006. *(Corresponding author: Cristina Catalá-Lahoz.)*

Cristina Catalá-Lahoz and José Capmany are with the Photonics Research Labs, iTEAM Research Institute, Universitat Politècnica de València, 46022 Valencia, Spain (e-mail: ccatala@iteam.upv.es; jcapmany@iteam.upv.es).

Moritz Merklein, Choon Kong Lai, and Benjamin J. Eggleton are with the University of Sydney Nano Institute (Sydney Nano), Institute of Photonics and Optical Science (IPOS), School of Physics, University of Sydney, Sydney, NSW 2006, Australia (e-mail: moritz.merklein@sydney.edu.au; choon.lai@sydney.edu.au; benjamin.eggleton@sydney.edu.au).

Duk-Yong Choi and Stephen J. Madden are with the Laser Physics Centre, Australian National University, Canberra, ACT 2601, Australia (e-mail: duk.choi@anu.edu.au; stephen.madden@anu.edu.au).

Color versions of one or more figures in this article are available at https://doi.org/10.1109/JLT.2025.3546728.

Digital Object Identifier 10.1109/JLT.2025.3546728

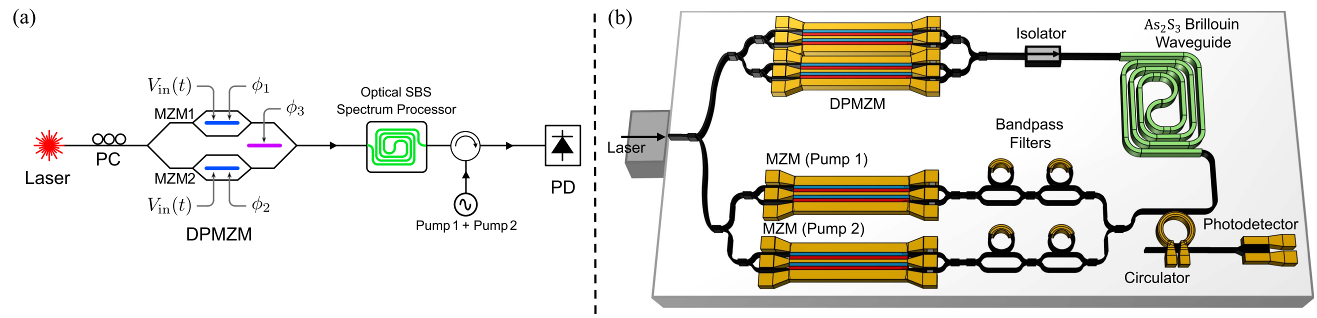

Fig. 1. (a) Schematic of the presented MPL using optical SBS spectrum processing for the linearization of a DPMZM. (b) Conceptual illustration of a chip-scale integrated SBS processor for a DPMZM linearization. PC, polarization controller; MZM, Mach-Zehnder modulator; DPMZM, dual-parallel Mach-Zehnder modulator; EDFA, erbium-doper fiber amplifier; PD, photodetector.

processing would ideally be achieved on a photonic chip to reduce overall space, cost, and power consumption.

Stimulated Brillouin Scattering (SBS) is ideal for this optical processing application due to its extremely narrow linewidth (around 30 MHz) [17], [18] and compatibility with chip-scale integration [19], [20]. SBS manifests itself as narrow gain and loss resonances when an optical pump wave is counter-propagated to an optical signal wave in a highly nonlinear waveguide [21]. By using two pump waves, the gain and loss resonances can be combined to precisely control the phase and amplitude of the optical carrier, enabling gain-transparent phase shifting. Initial demonstrations of this technique were performed in optical fibers [22], [23], and recent advancements have successfully implemented it using photonic chips [24].

In this work, we demonstrate the linearization of a DPMZM using SBS-based optical carrier processing, first induced by 4.46 km long single-mode fiber (SMF) spool, and then on a photonic chip with a 11.7 cm long chalcogenide waveguide. Using two individual counter-propagating pumps enables precise control of the amplitude and phase of the carrier via the induced SBS response. In the experimental results section, measurements for linearization effect over a 10 GHz bandwidth are shown, from around 2 GHz to 12 GHz, suppressing the IMD3 terms by over 25 dB, and measured SFDRs of up to 93.5 dB$\cdot$ Hz$^{2/3}$ and 88.13 dB$\cdot$ Hz$^{2/3}$ in optical fiber and the chip, respectively. The paper is outlined as follows: Section II introduces the theoretical operation principle of the technique used, Section III presents experimental results, first in fiber and then in a photonic chip, and finally Section IV provides some conclusions and discussion.

II. Operation Principle

The proposed MPL is shown in Fig. 1(a). It is composed of a DPMZM, where the MZMs in both arms are in a push-pull configuration. After modulation of the optical signal, we will use two SBS responses (pump 1 and pump 2) for processing the amplitude and phase of the optical carrier. For this modulation, we can find a pair of amplitude and phase values that, applied in the carrier band, will linearize the MPL upon photodetection. Fig. 1(b) shows a conceptual illustration of a chip-scale integrated SBS processor for this application, including a heterogeneous integration of an As $_2$ S_3 waveguide and other components such as modulators and tunable filters. This fully integrated system perfectly defines the long-term objective of this work, which aims to demonstrate that the use of Brillouin scattering can be useful to linearize a DPMZM, thus integrating the complete microwave photonic link. For the demonstrations, discrete elements and an integrated As_2S_3 waveguide have been used.

SBS is an optical nonlinearity that has gained interest for use in integrated MWP filters with fine spectral resolution [25]. This effect, driven by a third-order nonlinear acousto-optic interaction, features a narrow optical resonance linewidth (tens of MHz) due to the long phonon lifetime. SBS offers high spectral resolution and operates without a free spectral range (FSR), enabling a wide operational range. Additionally, the thermal stability of the Brillouin frequency shift can be much better than in a microring resonator (MRR).

The application of SBS as a phase-shifting mechanism [22], relies on counter-propagating a single sideband (SSB) modulated signal with two pump waves, where frequencies of the two pumps are symmetrically up and down-shifted with respect to the carrier frequency, close to the Brillouin frequency shift Ω_B. This results in a gain-transparent phase shift, as the two pumps are symmetric in frequency and power. The pump located at the left of the carrier will induce a loss response, while the pump located to the right of the carrier will induce a gain response on the carrier. Since the distance between the carrier and each pump is the same, and they have also the same power, the amplitudes of the loss and gain responses will have exactly the same transfer functions but with opposite signs, so they will counteract each other. In the case of the phase of each response, being contrary, they will add together resulting in a greater phase shift on the carrier.

The technique we apply, shown in Fig. 2(a), is based on the one mentioned above, but we use non-symmetrical pumps. Pump 1 acts as an SBS Stokes wave, and induces a loss resonance on the carrier, while Pump 2 acts as an SBS pump wave, inducing a gain resonance on the carrier. In this case, each pump will have a different frequency offset from the carrier, Ω_1 and Ω_2, and also different pump powers. This asymmetry results in the total amplitude response depending on the strength of the gain or loss induced by each pump, and a phase that will be the sum of the phases of the two SBS responses. In this way, by adjusting the frequency and power of each pump separately, we get more

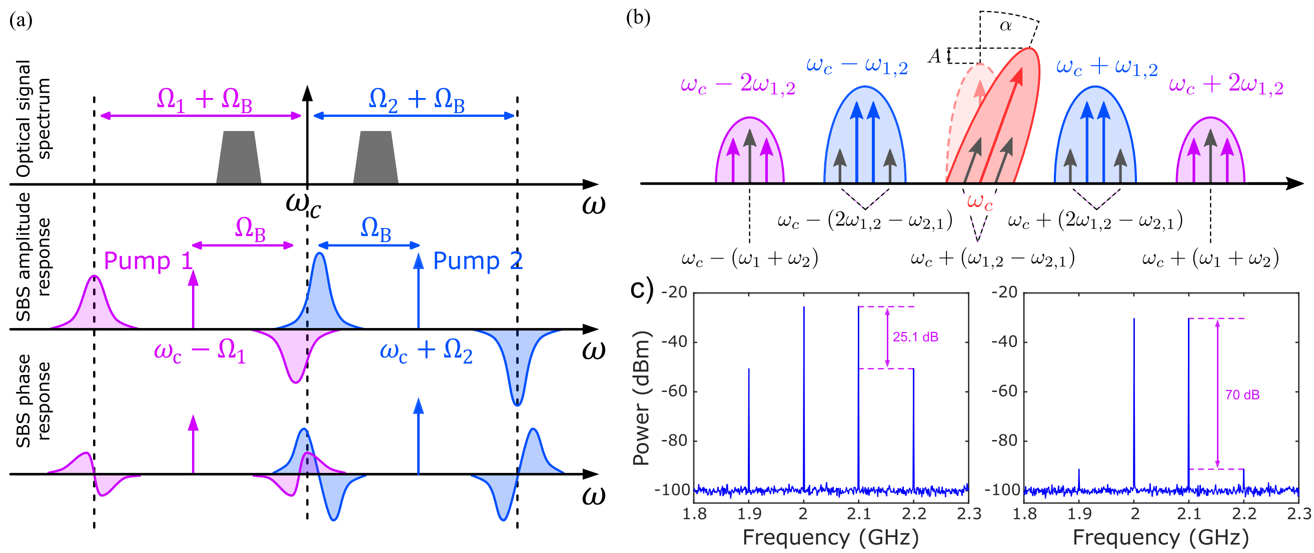

Fig. 2. (a) Operation principle for the SBS-based linearization method. (b) Optical spectrum after processing. (c) Simulated RF spectrum before and after linearization.

degrees of freedom to achieve the amplitude and phase shift needed to process the optical carrier.

SBS can be described in terms of its frequency response $|H_{\text{SBS}}(\Delta\omega)|e^{j\angle H_{\text{SBS}}}$ with

$$|H_{\text{SBS}}(\Delta\omega)| = \exp\left[\frac{G}{2}\frac{(\Gamma_{\text{B}}/2)^2}{\Delta\omega^2 + (\Gamma_{\text{B}}/2)^2}\right] \tag{1}$$

$$\angle H_{\text{SBS}}(\Delta\omega) = -\frac{G}{2}\Gamma_{\text{B}}\frac{\Delta\omega/2}{\Delta\omega^2 + (\Gamma_{\text{B}}/2)^2} \tag{2}$$

where Γ_{B} is the Brillouin linewidth and the G parameter is proportional to the SBS pump power as following

$$G = \frac{g_{\text{B}}}{A_{\text{ao}}}P_{\text{p}}L_{\text{eff}} = G_{\text{B}}P_{\text{p}}L_{\text{eff}}, \tag{3}$$

where g_{B} is the Brillouin gain coefficient in m/W (or G_{B} in m $^{-1}$ W^{-1}), A_{ao} is the acousto-optic effective area, and P_{p} is the pump power. Lastly, $L_{\text{eff}} = (1 - e^{-\alpha_{\text{M}}L_{\text{M}}})/\alpha_{\text{M}}$ is the effective length of the medium where SBS takes place, α_{M} is the attenuation coefficient of the medium and L_{M} is the medium length. Values of $G > 0$ corresponds to SBS gain centered at frequency $\Omega_p - \Omega_{\text{B}}$, while $G < 0$ corresponds to SBS loss centred at frequency $\Omega_p + \Omega_{\text{B}}$.

For simplicity in the equations, we use $Ae^{j\alpha}$ as the amplitude and phase of both SBS responses that are applied to the carrier.

In the proposed scheme in Fig. 1, we consider that both MZMs are modulated with a two-tone signal with angular frequencies ω_1 and ω_2 and amplitude V_{RF}, expressed as

$$V_{\text{in}}(t) = V_{\text{RF}}(\sin\omega_1 t + \sin\omega_2 t). \tag{4}$$

We can define the optical field at the output of a MZM as follows

$$E_{\text{MZM}_i}(t) = E_{\text{in}}(t)\left[e^{j\phi_i}e^{j\frac{\pi V_{\text{in}}(t)}{V_\pi}} + e^{-j\frac{\pi V_{\text{in}}(t)}{V_\pi}}\right], \tag{5}$$

where m is the modulation index, ϕ_i is the bias point of each MZM and $E_{\text{in}}(t) = \sqrt{P_{\text{in}}}e^{j\omega_c t}$. P_{in} and ω_c correspond to the power and frequency of the optical carrier. Then, the output optical field of the DPMZM $E_{\text{out}}(t)$ after the 3 dB coupler, is defined as

$$E_{\text{out}}(t) = \frac{\sqrt{2}}{2}\left[e^{j\phi_3}E_{\text{MZM}_1}(t) + E_{\text{MZM}_2}(t)\right] \tag{6}$$

being MZM_1 and MZM_2 the upper and lower Mach-Zehnder of the DPMZM and ϕ_3 is the phase induced by the third bias. Using the Jacobi-Anger expansion, we can develop (4) with

$$\begin{aligned} e^{jm\sin(\omega_1 t)} &= \sum_{n=-\infty}^{+\infty} J_n(m)e^{jn\omega_1 t} \\ e^{jm\sin(\omega_2 t)} &= \sum_{k=-\infty}^{+\infty} J_k(m)e^{jk\omega_2 t} \\ e^{-jm\sin(\omega_1 t)} &= \sum_{n=-\infty}^{+\infty} (-1)^n J_n(m)e^{jn\omega_1 t} \\ e^{-jm\sin(\omega_2 t)} &= \sum_{k=-\infty}^{+\infty} (-1)^k J_k(m)e^{jk\omega_2 t} \end{aligned} \tag{7}$$

where $J_n(m)$ refers to the n-th Bessel function of the first kind. The power of higher-order sidebands is quite small with a small RF input signal, so we only consider zero to second-order sidebands.

The output optical spectrum of the DPMZM is illustrated in Fig. 2(b), including the OCB, the ± 1 OSB and the ± 2 OSB. There are three pairs of main contributors to the IMD3. The first one is the beating of the optical carrier ω_c and $\omega_c \pm (2\omega_{1,2} - \omega_{2,1})$. The second one is the beating between ± 1 OSB of $\omega_c \pm \omega_{1,2}$ and ± 2 OSB of $\omega_c \pm 2\omega_{1,2}$. The third beating product is between $\omega_c \pm (\omega_{1,2} - \omega_{2,1})$ and $\omega_c \pm \omega_{1,2}$. The sum of the three beating products is the main part of the IMD3 terms.

Writing (4) as $E_{\text{MZM}_i}(t) = E_{\text{in}}(t)[e^{j\phi_i}S_+(t) + S_-(t)]$ and considering only zero to second order sidebands, $S_+(t)$ and $S_-(t)$ after processing by the SBS response can be expressed as

$$\begin{aligned} S_{\pm}(t) = & Ae^{j\alpha} J_0(m) J_0(m) \\ & + Ae^{j\alpha} J_{-1}(m) J_1(m) \left[e^{-j(\omega_1-\omega_2)t} + e^{j(\omega_1-\omega_2)t} \right] \\ & \pm J_0(m) J_1(m) \left(e^{j\omega_1 t} + e^{j\omega_2 t} \right) \\ & \pm J_{-1}(m) J_2(m) \left[e^{j(2\omega_1-\omega_2)t} + e^{-j(\omega_1-2\omega_2)t} \right] \\ & \pm J_{-1}(m) J_0(m) \left(e^{-j\omega_1 t} + e^{-j\omega_2 t} \right) \\ & \pm J_{-2}(m) J_1(m) \left[e^{-j(2\omega_1-\omega_2)t} + e^{j(\omega_1-2\omega_2)t} \right] \\ & + J_0(m) J_2(m) \left(e^{j2\omega_1 t} + e^{j2\omega_2 t} \right) \\ & + J_1(m) J_1(m) e^{j(\omega_1+\omega_2)t} \\ & + J_{-2}(m) J_0(m) \left(e^{-j2\omega_1 t} + e^{-j2\omega_2 t} \right) \\ & + J_{-1}(m) J_{-1}(m) e^{-j(\omega_1+\omega_2)t}, \end{aligned} \tag{8}$$

where $Ae^{j\alpha}$ is the amplitude and phase of the combination of the SBS gain and loss response applied to the OCB.

By using Taylor series expansion to the third order in m, the output photo-current of the photodetector, can be written as

$$\begin{aligned} I_{\text{PD}}(t) &= R_{\text{PD}} |E_{\text{out}}(t)|^2 \\ &= I_1 \sin(\omega_{1,2} t) + I_3 \sin(2\omega_{1,2} t - \omega_{2,1} t), \end{aligned} \tag{9}$$

where R_{PD} is the responsivity of the photodetector and I_1 and I_3 are the coefficients for fundamental and IMD3 frequencies, respectively. After small signal approximation and using $\phi_1 = \phi_2 = \pi/2$ and $\phi_3 = 0$ for the for the biases of the DPMZM, we can write both coefficients as

$$I_1 = -8\sqrt{2} m R_{\text{PD}} P_{\text{in}} A \cos\alpha, \tag{10}$$

$$I_3 = \sqrt{2} m^3 R_{\text{PD}} P_{\text{in}} (1 + 3A\cos\alpha). \tag{11}$$

From (10) shows that the IMD3 terms can be canceled by finding an amplitude A and a phase α applied to the OCB that satisfy $1 + 3A\cos\alpha = 0$. Note that under that condition the amplitude of the fundamental tones I_1 drops by 4.77 dB as $A\cos\alpha = 1/3$ in (9).

To verify the theoretical results, we simulated the MPL with a gain of $A = 5$ dB and a phase shift of $\alpha = 96^\circ$ applied to the OCB, so the SBS gain is considered to linearize the response. For simulation, we used an input optical power $P_{\text{in}} = 15$ dBm, an input RF power $P_{\text{RF}} = 5$ dBm, an RF half-wave voltage $V_\pi = 4$ V, the responsivity of the photodetector $R_{\text{PD}} = 0.45$ A/W and link losses of $L = 15$ dB. Fig. 2(c) shows the RF spectrum before linearization, where we obtain a 25.1 dB power ratio between fundamental and IMD3 tones. After linearization, we observe that the IMD3 components are suppressed by 44.9 dB, with a small reduction in the fundamental tones.

In a real scenario, the amplitude and phase may vary which makes it challenging to find the exact combination of values for the SBS processing. Fig. 3 shows the solution values between 0 and 1 for condition $1 + 3A\cos\alpha$. We can see that we can have a couple of degrees of error considering that values around zero still greatly reduce the IMD3 components. Additionally, to achieve greater control of this system, a single laser source is needed for both pump and probe sides to prevent relative drift, along with precise control over sideband position and power using tunable radio frequency sources.

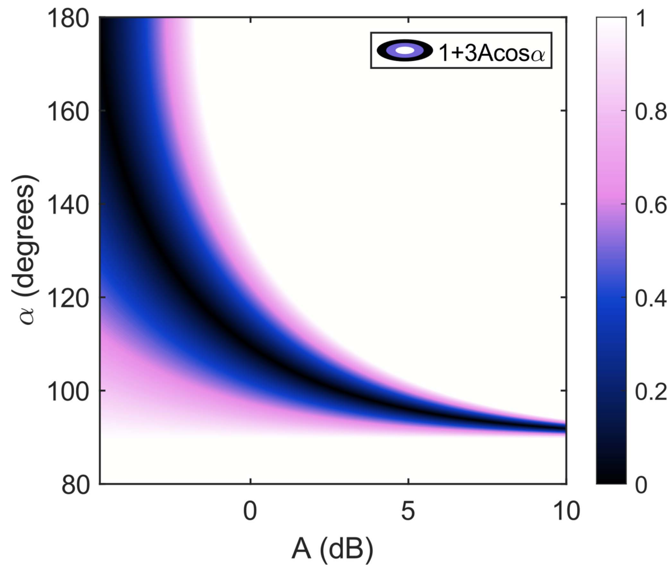

Fig. 3. Solutions in the range [0,1] for the multiplying factor in the IMD3 coefficient for different values of the amplitude and phase applied to the optical carrier.

III. Experimental Results

A. Single-Mode Fiber Experiment

The first demonstration was conducted using a single mode fiber (SMF) spool as a medium to generate the SBS response. The setup is shown in Fig. 4(a). A tunable DFB semiconductor laser diode (TeraXion PureSpectrum LM) was used, operating at 1550 nm with an output power of 18 dBm. A 3-dB coupler was used to split the laser power between the two branches of the setup. The upper branch generates a dual sideband modulation with the DPMZM (Sumitomo T· SBXH1.5.20PD-ADC), amplified by an erbium-doped fiber amplifier (EDFA1) before being transmitted through the fiber. The lower branch generates Pumps 1 and 2, by splitting the branch into two parallel paths with an MZM (Covega) in each arm, driven by separate signal generators (SG1 and SG2). The MZM outputs are filtered by optical bandpass filters (OBPF, Yenista XTM-50, and Alnair Labs BVF-300CL) to isolate single sidebands, creating RF tones that act as pumps. Both resulting tones are combined and amplified before counter-propagating through the fiber or the chip with the modulated carrier. Then, the output signal from the fiber, that is, the processed signal with the SBS responses, is photodetected.

Before linearizing the two-tone signal, we characterized the SBS responses using pumps driven by SG1 and SG2 to obtain a filter with the same features as we did for the simulation. In this case, the goal is to achieve around 5 dB gain and 96° degree phase shift to the carrier. To do so, we used the DPMZM as a single sideband (SSB) generator and a vector network analyzer

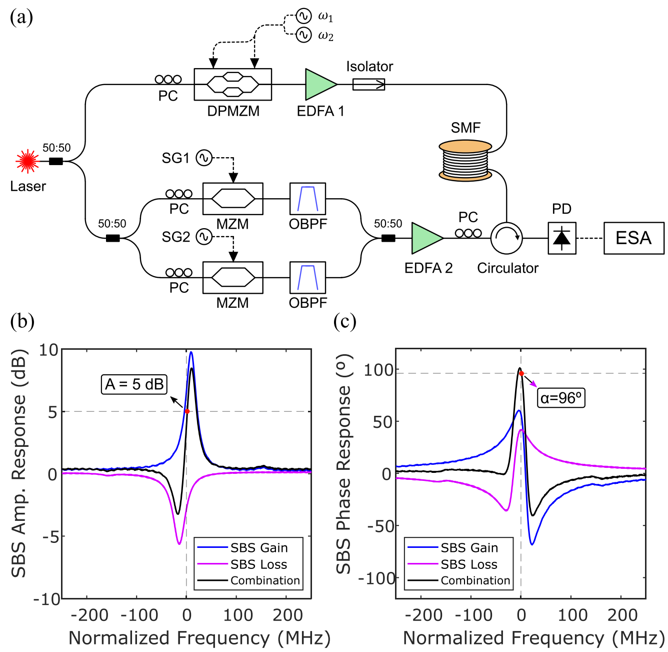

Fig. 4. (a) Experimental setup for the fiber experiment. (b) Measurement of the SBS gain and loss amplitude response and the combination of both applied for linearization. (c) Measurement of the SBS gain and loss phase response and the total phase applied for linearization. PC, polarization controller; DPMZM, dual-parallel Mach-Zehnder modulator; MZM, Mach-Zehnder modulator; SG, signal generator; EDFA, erbium-doped fiber amplifier; OBPF, optical band-pass filter; SMF, single-mode fiber; PD, photodetector; ESA, electrical spectrum analyzer.

(VNA) to measure the frequency response generated in the SMF. Fig. 4(b) and (c) show the measured SBS amplitude and phase responses generated by each pump, and the resulting response when both pumps are applied. The frequency and power of the two SBS pumps were exclusively controlled through the RF signal generators (SG). The signal generator used for the gain response was set to a frequency of 10.869 GHz with a 6.2 dBm pump power launched into the fiber. This power is measured right at the fiber input. For the loss response, the pump frequency was adjusted to 10.845 GHz with 3.8 dBm pump power. The fiber parameters are $L_{\mathrm{M}} = 4.46$ km, $\alpha_{\mathrm{M}} = 0.2$ dB/cm, $g_{\mathrm{B}} = 2.0 \times 10^{-11}$ m/W and $A_{\mathrm{ao}} \approx 78$ μm^2. Using the same carrier laser to generate both the pump and probe signals ensures that any drift in the laser wavelength affects both equally, significantly improving system stability.

Once we know the necessary parameters for achieving the desired gain and phase shift at the pump side, the linearization experiment is performed to verify the proposed method, based on the schematic in Fig. 4(a). Here we demonstrate the linearization of a DPMZM at two different RF frequencies 12 GHz and 2 GHz. In the first case, a two-tone signal with a central frequency of 12.53 GHz and a tone separation 100 MHz is generated by signal generators (HP 8673H SSG) and used to drive the DPMZM. For the second case, we used a central frequency of 2.05 GHz to demonstrate the operation at very low frequencies. In this system, the lower frequency limit (1.7 GHz) is set by the coupler used for feeding the RF signals, while the upper frequency limit (21.738 GHz) is due to the loss response generated by Pump 2 at 10.869 GHz. The processed optical signal by the

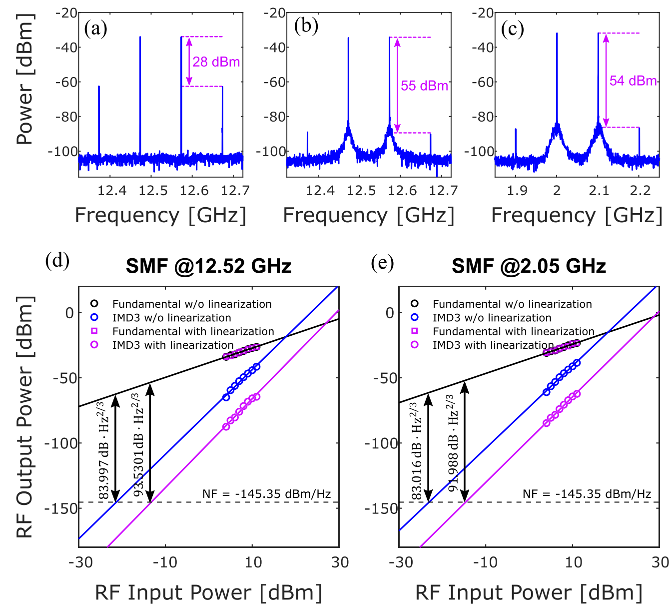

Fig. 5. (a) Measured electrical spectrum without linearization. (b) Linearized spectrum at 12.52 and (c) 2.05 GHz using fiber. (d) Measured SFDR of the MPL without and with linearization at 12.52 and (e) 2.05 GHz using fiber.

previous SBS response is then sent to a photodetector (Finisar HPDV2120R) and measured in an electric spectrum analyzer (ESA). The previous technique [16] was limited to a minimum modulation frequency of 5 GHz due to the wide bandwidth of the optical spectral shaper used. This method allows modulation at lower frequencies as the Brillouin linewidth is $\Gamma_{\mathrm{B}} \approx 60$ MHz.

The measured spectrum without the SBS processing is shown in Fig. 5(a), i.e., with SG1 and SG2 turned off. Results of linearized power spectra are shown in Fig. 5(b) and (c) at 12.53 and 2.05 GHz respectively, showing a suppression of 27 dB in both frequency bands compared to the unprocessed spectrum. SFDR measurements are shown in Fig. 5(d) and (e) for both frequencies, where we achieve values of 93.5 and 92 dB$\cdot$ Hz$^{2/3}$. This means an improvement of around 9 dB.

B. Chalcogenide Chip Experiment

We then replaced the fiber with a 11.7-cm-long chalcogenide (As_2S_3) spiral rib waveguide, with a cross-section of 2.6 μm $\times$ 960 nm, 33% etch depth, and 0.4 dB/cm propagation loss. Vertical tapers were used to transition from the chalcogenide waveguide to Germanosilicate waveguides at both ends of the chip; these Germanosilicate waveguides minimize the refractive index mismatch between the chip and optical fiber and reduce the backreflection [26]. Whereas the waveguide is optically multi-moded, we ensure that light is coupled into the quasitransverse electric (TE) mode by minimizing the overall loss. The acoustic mode is guided in the waveguide core via total internal reflection due to a contrast in the acoustic impedance. The light was coupled into the chip using ultra-high numerical aperture (UHNA-3) fiber, with index matching fluid between the fiber and chip interface to maximize coupling efficiency and further reduce back-reflection.

TABLE I
PERFORMANCE COMPARISON WITH THE STATE-OF-THE-ART LINEARIZATION TECHNIQUES USING OPTICAL PROCESSING

Modulator	Linearization Technique	IMD3 Suppression (dB)	SFDR (dB·Hz$^{2/3}$)	SFDR Improvement (dB)
PM [9]	Integrated ring resonators	21.7	106.9	1.1
PM [5]	Multi-functional integrated MWP circuit	28.7	123.6	19.8
MZM [8]	WaveShaper programmable filter	34.1	114.3	14.7
DPMZM [15]	Stimulated Brillouin Scattering	23.7	108.0	10.3
DPMZM [16]	WaveShaper programmable filter	17	86.92	3
DPMZM (This work)	On-chip stimulated Brillouin Scattering	27	88.13	4.5

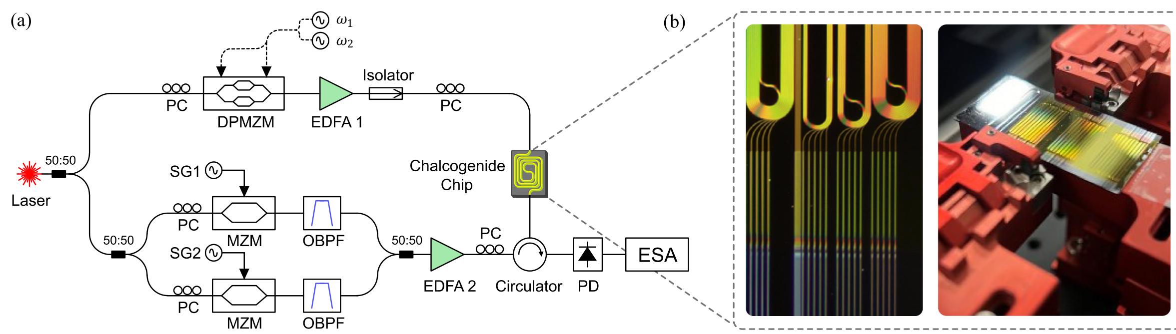

Fig. 6. (a) Experimental setup for the on-chip SBS linearization experiment. (b) Photo of the chalcogenide chip mounted on a coupling stage with a zoom-in on the spiral rib waveguides. PC, polarization controller; DPMZM, dual-parallel Mach-Zehnder modulator; MZM, Mach-Zehnder modulator; SG, signal generator; EDFA, erbium-doped fiber amplifier; OBPF, optical band-pass filter; SMF, single-mode fiber; PD, photodetector; ESA, electrical spectrum analyzer.

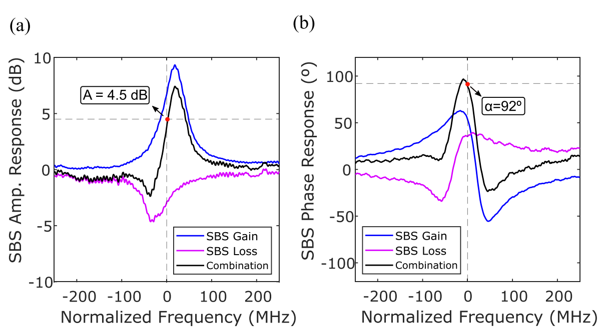

Fig. 7. (a) Measurement of the on-chip SBS gain and loss amplitude response and the combination of both applied for linearization. (b) Measurement of the on-chip SBS gain and loss phase response and the total phase applied for linearization.

The setup used is shown in Fig. 6(a) and (b) shows detailed photographs of the chip layout (which contains spirals with different lengths) and the coupling station used for the measurements.

For the chalcogenide chip, the Brillouin frequency shift is $\Omega_B = 7.72$ GHz. Fig. 7(a) and (b) show the characterized SBS responses in amplitude and phase. In this case, we can achieve around 4.5 dB gain and 92° phase shift due to the higher losses of the chip. The signal generator used for the gain response was set to a frequency of 7.738 GHz with a 30.4 dBm pump power launched into the facet of the waveguide. For the loss response, the pump frequency was adjusted to 7.69 GHz with 28.2 dBm pump power. The waveguide parameters are $L_M = 11.7$ cm, $\alpha_M = 0.2$ dB/cm and $G_B = 344$ m^{-1} W^{-1}.

Very similar suppression values are obtained in the chip, shown in Fig. 8(a) and (b). Total insertion losses of the chip are 11.5 dB, resulting in a higher noise floor due to the need

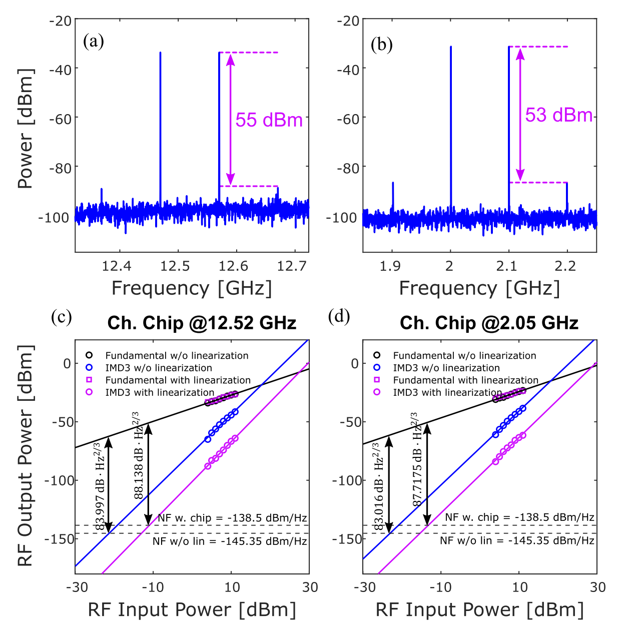

Fig. 8. (a) Linearized spectrum at 12.52 and (b) 2.05 GHz using the chalcogenide (ch.) chip. (c) Measured SFDR of the MPL without and with linearization at 12.52 and (d) 2.05 GHz the ch. chip.

for additional amplification to compensate for the loss. SFDR measurements are shown in Fig. 8(c) and (d), with improvements of around 4.5 dB and SFDR values of 88.13 and 87.71 dB·Hz$^{2/3}$.

IV. CONCLUSION

Our results, showing more than 25 dB suppression of IMD3 components, demonstrate the possibility of linearizing the response of a DPMZM using SBS as a very narrow response for processing the optical carrier only, and hence allowing for the sidebands to be close to the carrier. Furthermore, our measurements using a chalcogenide chip are an important step toward fully integrating the system into a single chip, further reducing losses and footprint [27], and improving the received power and noise floor level, and hence SFDR.

Compared to other similar approaches (Table I), our results in terms of IMD3 suppression show the best result for a DPMZM using optical processing, and similar results to some performed for phase modulation. Regarding SFDR, we obtain low values compared to the rest of the works due to the link performance, but we obtain good values in terms of total improvement, compared with some of the on-chip processing demonstrations.

Brillouin-based photonic processing for MWP faces persistent challenges, primarily due to amplification noise that significantly degrades the signal. Developing low-noise or noise-free Brillouin signal processing remains a fundamental goal. Efforts have been made to investigate the integration of SBS onto CMOS-compatible silicon platforms, showing a phase shifter directly in a suspended silicon waveguide, which together with the availability of silicon modulators could be the basis of a monolithic approach [28]. While this strategy shows promise, silicon faces inherent limitations, such as suboptimal electro-optic modulator performance and nonlinear absorption, which restrict its effectiveness in certain applications. Recent demonstrations of SBS in other platforms like lithium niobate [29], thin-film lithium niobate [30] or silicon nitride [31], with superior acousto-optic coupling and electromechanical transduction efficiency, as well as the heterogeneous integration of chalcogenide glasses like As_2S_3 [18], offer promising pathways.

References

[1] J. Capmany and D. Novak, “Microwave photonics combines two worlds,” *Nature Photon.*, vol. 1, pp. 319–330, Jun. 2007.

[2] J. Yao, “Microwave photonics,” *J. Lightw. Technol.*, vol. 27, no. 3, pp. 314–335, Feb. 2009.

[3] D. Marpaung, J. Yao, and J. Capmany, “Integrated microwave photonics,” *Nature Photon.*, vol. 13, pp. 80–90, Jan. 2019.

[4] C. H. Cox, E. I. Ackerman, G. E. Betts, and J. L. Prince, “Limits on the performance of RF-over-fiber links and their impact on device design,” *IEEE Trans. Microw. Theory Techn.*, vol. 54, no. 2, pp. 906–920, Feb. 2006.

[5] G. Liu, K. Ye, O. Daulay, Q. Tan, H. Yu, and D. Marpaung, “Linearized integrated microwave photonic circuit for filtering and phase shifting,” *APL Photon.*, vol. 8, 2023, Art. no. 051303.

[6] O. Daulay, R. Botter, and D. Marpaung, “On-chip programmable microwave photonic filter with an integrated optical carrier processor,” *OSA Continuum*, vol. 3, no. 8, pp. 2166–2174, Aug. 2020.

[7] E. I. Ackerman, “Broad-band linearization of a Mach-Zehnder electrooptic modulator,” *IEEE Trans. Microw. Theory Techn.*, vol. 47, no. 12, pp. 2271–2279, Dec. 1999.

[8] J. Lin et al., “Intermodulation distortion suppression for intensity-modulated analog fiber-optic link incorporating optical carrier band processing,” *Opt. Exp.*, vol. 21, pp. 23433–23440, Oct. 2013.

[9] G. Liu, G. Liu, O. Daulay, Q. Tan, H. Yu, and D. Marpaung, “Linearized phase modulated microwave photonic link based on integrated ring resonators,” *Opt. Exp.*, vol. 28, pp. 38603–38615, Dec. 2020.

[10] Y. Zhou et al., “Linearity characterization of a dual-parallel silicon Mach-Zehnder modulator,” *IEEE Photon. J.*, vol. 8, no. 6, Dec. 2016, Art. no. 7805108.

[11] G. Zhu, W. Liu, and H. R. Fetterman, “A broadband linearized coherent analog fiber-optic link employing dual parallel Mach-Zehnder modulators,” *IEEE Photon. Technol. Lett.*, vol. 21, no. 21, pp. 1627–1629, Nov. 2009.

[12] S. Li, X. Zheng, H. Zhang, and B. Zhou, “Highly linear radio-over-fiber system incorporating a single-drive dual-parallel Mach-Zehnder modulator,” *IEEE Photon. Technol. Lett.*, vol. 22, no. 24, pp. 1775–1777, Dec. 2010.

[13] W. Jiang et al., “A linearization analog photonic link with high third-order intermodulation distortion suppression based on dual-parallel Mach-Zehnder modulator,” *IEEE Photon. J.*, vol. 7, no. 3, Jun. 2015, Art. no. 7902208.

[14] Y. Gu and J. Yao, “Microwave photonic link with improved dynamic range through π phase shift of the optical carrier band,” *J. Lightw. Technol.*, vol. 37, no. 3, pp. 964–970, Feb. 2019.

[15] W. Zhu et al., “Dynamic range improvement of a microwave photonic link based on Brillouin processing,” *IEEE Photon. Technol. Lett.*, vol. 28, no. 23, pp. 2681–2684, Dec. 2016.

[16] L. Torrijos-Moran, C. Catala-Lahoz, D. Perez-Lopez, L. Xu, W. Tianxiang, and D. Perez-Galacho, “Linearization of a dual-parallel Mach-Zehnder modulator using optical carrier band processing,” *J. Lightw. Technol.*, vol. 41, no. 10, pp. 2969–2975, May 2023.

[17] D. Benito, M. J. Garde, and A. Loayssa, “Optical carrier Brillouin processing of microwave photonic signals,” *Opt. Lett.*, vol. 25, pp. 1234–1236, Sep. 2000.

[18] M. Garrett et al., “Integrated microwave photonic notch filter using a heterogeneously integrated Brillouin and active-silicon photonic circuit,” *Nature Commun.*, vol. 14, Nov. 2023, Art. no. 7544.

[19] B. J. Eggleton, C. G. Poulton, P. T. Rakich, M. J. Steel, and G. Bahl, “Brillouin integrated photonics,” *Nature Photon.*, vol. 13, pp. 664–677, Aug. 2019.

[20] G. Neijts et al., “On-chip stimulated Brillouin scattering via surface acoustic waves,” *APL Photon.*, vol. 9, 2024, Art. no. 106114.

[21] D. Marpaung, M. Pagani, B. Morrison, and B. J. Eggleton, “Nonlinear integrated microwave photonics,” *J. Lightw. Technol.*, vol. 32, no. 20, pp. 3421–3427, Oct. 2014.

[22] A. Loayssa, S. Galech, and F. Lahoz, “Broadband microwave photonic phase-shifter based on stimulated Brillouin scattering,” in *Proc. IEEE LEOS Annu. Meeting Conf.*, 2005, pp. 839–840.

[23] M. Pagani, D. Marpaung, and B. J. Eggleton, “Ultra-wideband microwave photonic phase shifter with configurable amplitude response,” *Opt. Lett.*, vol. 39, pp. 5854–5857, Oct. 2014.

[24] M. Pagani, D. Marpaung, D. Y. Choi, S. J. Madden, B. Luther-Davies, and B. J. Eggleton, “Tunable wideband microwave photonic phase shifter using on-chip stimulated Brillouin scattering,” *Opt. Exp.*, vol. 22, pp. 28810–28818, Nov. 2014.

[25] R. Pant et al., “On-chip stimulated Brillouin scattering,” *Opt. Exp.*, vol. 19, pp. 8285–8290, Apr. 2011.

[26] C. K. Lai et al., “Hybrid chalcogenide-germanosilicate waveguides for high performance stimulated Brillouin scattering applications,” *Adv. Funct. Mater.*, vol. 32, Jan. 2022, Art. no. 2105230.

[27] C. K. Lai, M. Merklein, A. C. Bedoya, and B. J. Eggleton, “Heterogeneous and hybrid integration for Brillouin microwave photonics,” *Adv. Phys.: X*, vol. 9, 2024, Art. no. 2360598.

[28] L. McKay et al., “Brillouin-based phase shifter in a silicon waveguide,” *Optica*, vol. 6, no. 7, pp. 907–913, Jul. 2019.

[29] C. C. Rodrigues, R. O. Zurita, T. P. M. Alegre, and G. S. Wiederhecker, “Stimulated Brillouin scattering by surface acoustic waves in lithium niobate waveguides,” *J. Opt. Soc. Amer. B*, vol. 40, no. 5, pp. D56–D63, May 2023.

[30] K. Ye et al., “Surface acoustic wave Brillouin scattering in thin-film lithium niobate waveguides,” presented at the Conf. Lasers Electro-Opt.: Sci. Innov., Charlotte, NC, USA, May 5–10, 2024, Paper STu4P.3.

[31] F. Gyger et al., “Observation of stimulated Brillouin scattering in silicon nitride integrated waveguides,” *Phys. Rev. Lett.*, vol. 124, Jan. 2020, Art. no. 013902.

Cristina Catalá-Lahoz received the B.Sc. and M.Sc. degrees in telecommunications engineering from the Universitat Politècnica de València, Valencia, Spain, where she currently working toward the Ph.D. degree in telecommunications, focusing on the design and development of programmable photonic integrated circuits for high-performance microwave photonic systems, filtering, and communications with Photonics Research Labs, Institute of Telecommunications and Multimedia Applications.

Moritz Merklein received the Ph.D. degree from the University of Sydney, Sydney, NSW, Australia, in 2018. He is currently a Senior Research Fellow with the University of Sydney, and a Team Leader with Jericho Smart Sensing Laboratory. His research was the recipient of the several awards, including the Rita and John Cornforth Graduate Medal 2019, Royal Society of NSW Jak Kelly Award 2017, and Australian Institute of Physics NSW Medal for Postgraduate Excellence 2017. He was also the recipient of a 2020 Eureka Prize.

Choon Kong Lai received the dual Ph.D. degrees from the Australian National University, Canberra, Australia, and from the University of Malaya, Kuala Lumpur, Malaysia, in 2021, respectively. He is currently a Postdoctoral Research Associate with the University of Sydney, Sydney, NSW, Australia. His research interests integrated photonics, encompassing hybrid and heterogeneous integration, chalcogenide glasses, Brillouin scattering, microwave photonics, phase-change materials, and graphene oxide photonics.

Duk-Yong Choi received the Ph.D. degree in materials science and engineering from Seoul National University, Korea, in 1998. He was with Samsung Electronics, South Korea, as Process Engineer, for a period of 6.5 years in Industry. In 2005, he joined the Australian National University, Canberra, ACT, Australia. His research interests include silicon photonics, chalcogenide photonics, quantum photonics, and nanophotonic.

Stephen J. Madden received the B.Sc. degree in electronic engineering and the Ph.D. degree in integrated optics from Imperial College London, London, U.K., in 1985 and 1989, respectively. He is currently an Associate Professor and a Fellow with Laser Physics Centre, Australian National University (ANU), Canberra, ACT, Australia. He has spent most of his career in industry. In 1991, he joined Telstra Research Laboratories, Melbourne, VIC, Australia. In 1997, he became the Director of Research with ADC Telecommunications, Minneapolis, MN, USA, before leaving to become VP Engineer with Sparkolor Corporation, Santa Clara, CA, USA, in 2001. He has authored or coauthored more than 200 papers.He led a Research with CUDOS, a research consortium between seven Australian universities, into photonics devices.

Benjamin J. Eggleton (Fellow, IEEE) received the bachelor's degree (with Hons.) in science and the Ph.D. degree in physics from the University of Sydney, Sydney, Australia, in 1992 and 1996, respectively.

In 1996, he joined Bell Laboratories, Lucent Technologies, Murray Hill, NJ, USA, as a Postdoctoral Member of Staff and later transitioned to the Department of Optical Fiber Research. In 2000, he was appointed Research Director with Specialty Fiber Business Division, where he led forward-looking research to support Lucent Technologies' optical fiber device business. In 2003, he returned to the University of Sydney, as a Professor with the School of Physics. From 2003 to 2017, he was an Australian Research Council (ARC) Federation Fellow, Laureate Fellow, and the Director of the ARC Centre for Ultrahigh-Bandwidth Devices for Optical Systems (CUDOS). From 2018 to 2022, he was the Director with the University of Sydney Nano Institute (Sydney Nano). He also holds the role of Pro Vice-Chancellor (Research) and is the Co-Director of the NSW Smart Sensing Network (NSSN).

He has authored or coauthored of more than 520 journal publications, with more than 30,000 citations (Web of Science). His research interests include nonlinear optics, all-optical signal processing, microwave photonics and smart sensing. He was the recipient of the numerous awards which include the 2011 Walter Boas Medal from the Australian Institute of Physics, 2007 Pawsey Medal from the Australian Academy of Science, 2004 Malcolm McIntosh Prize for Physical Scientist of the Year, 2003 International Commission on Optics Prize, 1998 Adolph Lomb Medal from the Optical Society, Distinguished Lecturer Award from the IEEE/Lasers and Electro-Optics Society, and Research and Development 100 Award. From 2008 to 2010, he was President of the Australian Optical Society. He is also the Editor-in-Chief of APL Photonics. He is a Fellow of the Optical Society (Optica), IEEE Photonics Society, SPIE, the Australian Academy of Science, and the Australian Academy of Technological Sciences and Engineering.

José Capmany (Fellow, IEEE) was born in Madrid, Spain. He received the Ingeniero de Telecomunicacion degree from the Universidad Politécnica de Madrid (UPM), Madrid, Spain, in 1987, the Licenciado en Ciencias Físicas degree in 2009, the Ph.D. degree in electrical engineering, the Ph.D. degree in quantum physics from UPM, in 1991 and 2010, respectively, and the the Ph.D. degree from the Universidad de Vigo, Vigo, Spain, in 1991.

Since 1991, he has been with the Departamento de Comunicaciones, Universidad Politècnica de València (UPV), Valencia, Spain, where he started the activities on optical communications and photonics, founding the Photonics Research Labs Group. From 1992 to 1995, he was an Associate Professor, and has been a Full Professor of photonics and optical communications since 1996. From 1991 to 1996, he was the Vice-Dean at the Telecommunications Engineering School, UPV, and the Deputy Head of the Communications Department from 1997 to 2005. From 2005 to 2016, he was the Director of the Research Institute of Telecommunications and Multimedia Applications (iTEAM), UPV. He has authored or coauthored more than 550 papers in international refereed journals and conferences. His research interests include wide range of subjects related to optical communications including microwave photonics, integrated optics, optical signal processing, fiber Bragg gratings, and more recently quantum cryptography and quantum-photonic information processing.

He is also the Founder and the Chief Innovation Officer with spin-off Company VLC Photonics, Valencia, Spain, dedicated to the design of photonic integrated circuits, EPHOOX, Valencia, dedicated to MWP instrumentation, and iPronics Programmable Photonics S.L., Valencia, dedicated to integrated programmable photonic circuits. He was a reviewer for more than 30 SCI journals in the field of photonics and telecommunications. From 2008 to 2010, he was a member of the IEEE Photonics Society Board of Governors, and a Distinguished Lecturer, from 2013 to 2014. In 2015, he was the General Chair for the 41st European Conference on Optical Communications (ECOC), Valencia, and for the IEEE International Topical Meeting on Microwave Photonics in 2009. He was a member of the Technical Program Committees of more than 50 international conferences in the field of photonics including ECOC, Optical Fiber Conference, Integrated Optics and Optical Communications Conference, CLEO Europe, and the Optoelectronics and Communications Conference. From 2010 to 2016, he was an Associate Editor for IEEE PHOTONICS TECHNOLOGY LETTERS and IEEE JOURNAL OF LIGHTWAVE TECHNOLOGY, from 2016 to 2018. He has also been a Guest Editor of the IEEE JOURNAL OF SELECTED TOPICS IN QUANTUM ELECTRONICS, IEEE TRANSACTIONS ON MICROWAVE THEORY AND TECHNIQUES, and *Optics Express* feature issue on microwave photonics. He has been the Editor-in-Chief of the IEEE JOURNAL OF SELECTED TOPICS IN QUANTUM ELECTRONICS. He was recipient of the 2012 King James I Prize Laureate on Novel Technologies, Highest Scientific Distinction in Spain, for his outstanding contributions to the field of microwave photonics, two European Research Council Advanced Grants, in 2016 and 2023, and the Extraordinary Doctorate Prize of the Universidad Politecnica de Madrid, 1992. He is a Fellow of the Optical Society of America.